ISSN 1392-1207. MECHANIKA. Vol. 32, No. 2, 2026: 107–115

Research on Dynamic Load Identification Based on the Newmark-β Method and Novel Iterative Regularization Strategy

Hongqiu LI*, Jinhui JIANG, M Shadi MOHAMED*****

**Mechatronic Engineering College, Jinling Institute of Technology, Nanjing 211169, China, E-mail: lihongqiu@jit.edu.cn*

***State Key Laboratory of Mechanics and Control for Aerospace structures, Nanjing University of Aeronautics and Astronautics, Nanjing 210016, China, E-mail: jiangjinhui@nuaa.edu.cn*

****Institute for Infrastructure and Environment, Heriot-Watt University, Edinburgh EH14 4AS, UK, E-mail:M.S.Mohamed@hw.ac.uk*

https://doi.org/10.5755/j02.mech.42732

1. Introduction

Accurate identification of structural dynamic loads is critical for structural design optimization, health monitoring, and fault diagnosis. Direct measurement of dynamic loads is often impractical, the primary approach is to deduce the excitation based on structural dynamic responses [1]. Despite significant advancements, challenges persist in addressing ill-posedness, noise interference, and multi-source uncertainties in dynamic load identification [2-3].

Traditional dynamic load identification methods can be broadly classified into time-domain and frequency-domain approaches. Frequency-domain methods simplify the convolution integral but struggle with non-stationary loads and resonance effects. Qin Y et al. [4] developed an innovative dynamic load localization method combining symbolic computation in the complex frequency response function (FRF) domain with genetic algorithm optimization, effectively eliminating amplitude and phase variables. In contrast, Time-domain methods reconstruct loads based on convolution relationships, making them more suitable for transient and impact loads. Kulkarni et al. [5] proposed an algorithm for accurate impact force identification in spacecraft structures using time-domain spectral finite element modeling, requiring fewer measured responses than conventional methods. Yue K [6] developed a Bayesian approach for the simultaneous online estimation of vehicle loads, positions, and bridge structural parameters using only strain measurements. Pourzeynali S [7] derived an explicit form of the Newmark-β method which can identify the moving loads and structural damage simultaneously. Cheng Y et al. [8] derived the Newmark-β method in modal space and combined it with the state-space method (SSM) to establish a load identification model, significantly reducing the dimensionality of the transfer matrix.

To address ill-posedness, various regularization strategies have been proposed. Yu X et al. [9] developed a maximumly weighted iteration method to enhance the stability of solving inverse dynamic problems. Carevic A et al. [10] used the Tikhonov regularization with different algorithms for choosing the regularization parameter that provides optimal balance, a solution neither overregularized nor underregularized. Wang L et al. [11] employed a set-theoretical wavelet transform with layered noise reduction to improve robustness in multi-source uncertain systems. The Least Squares QR Decomposition (LSQR) method has become an important tool for solving ill-posed inverse problems due to its advantages in handling large sparse systems. Martin H [12] proposed a hybrid regularization algorithm, which first transforms the system into a small bidiagonal system based on the Lanczos process, and then uses truncated singular value decomposition (TSVD) to stabilize the iterative process, which has strong stability. Baglama J [13] proposed the augmented LSQR iterative algorithm, which enhances the Krylov subspace by harmonizing the Ritz vector, enabling rapid convergence of the iteration. Asgari Z et al. [14] proposed a restart LSQR algorithm, which is suitable for solving large-scale ill posed problems and reduces the storage space of matrices during the iteration process.

With the advancement of artificial intelligence, the integration of data-driven approaches and physical mechanisms has emerged as a new research focus. Subrata Saha [15] proposed a method for calculating the dynamic loads on a vibrating pipework in a process plant based on the Theory of Inverse Problems and physics-informed neural networks (PINN). Cui W et al. [16] (2023) introduced Convolutional Neural Networks (CNN) for reconstruction of unknown load intervals, using data-driven identification methods to solve the problem of ill conditioned matrices and parameter uncertainty in physical models.

Despite substantial progress, challenges remain in addressing algorithmic ill-posedness and improving identification accuracy. This paper focuses on the Newmark-β time-domain algorithm for dynamic load identification in continuous systems. After analyzing its stability, we propose suitable parameter selection ranges. To mitigate the algorithm's ill-posedness, we introduce an improved hybrid LSQR algorithm. At each iteration step, the computed response from the hybrid LSQR algorithm is compared with the measured response, and the algorithm is dynamically adjusted based on their discrepancy. Simulation case demonstrate that this method exhibits enhanced stability and computational accuracy. Furthermore, we propose an augmented hybrid LSQR algorithm, which incorporates prior knowledge of the load to further improve convergence speed and identification precision. Finally, using a simply supported beam as an example, the reliability and accuracy of the hybrid LSQR correction algorithm in identifying periodic loads are verified through simulation and experimentation.

2. Dynamic Load Identification Algorithm Based on Explicit Newmark-β Method

One multi-degree-freedom system is shown in Fig. 1, where m_i, k_i, and c_i represent mass, stiffness, and

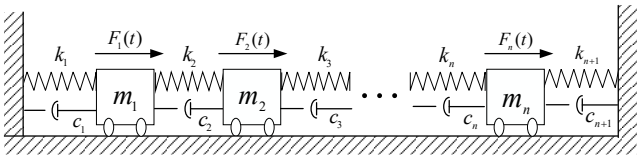

Fig. 1 Multi-degree-freedom spring damping system

damping respectively. $F_i(t)$ is the external load. If the actual structure is a continuum system, modal truncation can be used to reduce the system order. Assuming the modal truncation order is r, the dynamic equations of a continuous system can be transformed into a finite number of independent equations in modal space. After normalizing the modal mass, we obtain [17]:

$$\ddot{\boldsymbol{q}}(t)+\boldsymbol{C}\dot{\boldsymbol{q}}(t)+\boldsymbol{K}\boldsymbol{q}(t)=\boldsymbol{f}(t), \tag{1}$$

where, $\boldsymbol{q}(t) = \{q_1(t), q_2(t), \ldots, q_r(t)\}^T$ is the modal coordinate vector; $\dot{\boldsymbol{q}}(t)$ is velocity vector and $\ddot{\boldsymbol{q}}(t)$ is acceleration vector; $\boldsymbol{f}(t)$ is modal force; and

$$\boldsymbol{C}=\begin{bmatrix} 2\xi_1\omega_1 & 0 & \cdots & 0 \\ 0 & 2\xi_2\omega_2 & \cdots & 0 \\ \vdots & \vdots & \ddots & \vdots \\ 0 & 0 & \cdots & 2\xi_r\omega_r \end{bmatrix},$$

$$\boldsymbol{K}=\begin{bmatrix} \omega_1^2 & 0 & \cdots & 0 \\ 0 & \omega_2^2 & \cdots & 0 \\ \vdots & \vdots & \ddots & \vdots \\ 0 & 0 & \cdots & \omega_r^2 \end{bmatrix}. \tag{2}$$

Among them, $\omega_1, \omega_2, \ldots, \omega_r$ are the natural frequency of the system, and $\xi_1, \xi_2, \ldots, \xi_r$ are the modal damping coefficients of the system.

We assume that the structural responses vary linearly in the time interval $[t_i \ \ t_{i+1}]$ with the time step Δt. Therefore, the modal responses of multi-degree-freedom system can be obtained by implicit Newmark-β method [17]:

$$\begin{bmatrix} \boldsymbol{q}(t_i) \\ \dot{\boldsymbol{q}}(t_i) \\ \ddot{\boldsymbol{q}}(t_i) \end{bmatrix} = \sum_{j=0}^{i-1} \begin{bmatrix} \boldsymbol{A}_d & \boldsymbol{A}_v & \boldsymbol{A}_a \\ \boldsymbol{B}_d & \boldsymbol{B}_v & \boldsymbol{B}_a \\ \boldsymbol{C}_d & \boldsymbol{C}_v & \boldsymbol{C}_a \end{bmatrix}^j \begin{bmatrix} \boldsymbol{A}_0 \\ \boldsymbol{B}_0 \\ \boldsymbol{C}_0 \end{bmatrix} \boldsymbol{f}(t_{i-j}) + \\ + \begin{bmatrix} \boldsymbol{A}_d & \boldsymbol{A}_v & \boldsymbol{A}_a \\ \boldsymbol{B}_d & \boldsymbol{B}_v & \boldsymbol{B}_a \\ \boldsymbol{C}_d & \boldsymbol{C}_v & \boldsymbol{C}_a \end{bmatrix}^i \begin{bmatrix} \boldsymbol{q}(t_0) \\ \dot{\boldsymbol{q}}(t_0) \\ \ddot{\boldsymbol{q}}(t_0) \end{bmatrix}, \tag{3}$$

in which,

$$\begin{aligned} \boldsymbol{A}_0 &= \left(\frac{1}{\beta(\Delta t)^2}\boldsymbol{I} + \frac{\gamma}{\beta\Delta t}\boldsymbol{C} + \boldsymbol{K} \right)^{-1}, \\ \boldsymbol{A}_d &= \boldsymbol{A}_0 \left[\frac{1}{\beta(\Delta t)^2}\boldsymbol{I} + \frac{\gamma}{\beta\Delta t}\boldsymbol{C} \right], \\ \boldsymbol{A}_v &= \boldsymbol{A}_0 \left[\frac{1}{\beta\Delta t}\boldsymbol{I} + \left(\frac{\gamma}{\beta}-1\right)\boldsymbol{C} \right], \\ \boldsymbol{A}_a &= A_0 \left[\left(\frac{1}{2\beta}-1\right)\boldsymbol{I} + \frac{\Delta t}{2}\left(\frac{\gamma}{\beta}-2\right)\boldsymbol{C} \right], \end{aligned} \tag{4}$$

$$\begin{aligned} \boldsymbol{B}_0 &= \frac{\gamma}{\beta\Delta t}\left(\frac{1}{\beta(\Delta t)^2}\boldsymbol{I} + \frac{\gamma}{\beta\Delta t}\boldsymbol{C} + \boldsymbol{K} \right)^{-1}, \\ \boldsymbol{B}_d &= -\boldsymbol{B}_0\boldsymbol{K}, \\ \boldsymbol{B}_v &= \boldsymbol{B}_0 \left[\left(\frac{\beta\Delta t}{\gamma} - \Delta t\right)\boldsymbol{K} + \frac{1}{\gamma\Delta t}\boldsymbol{I} \right], \\ \boldsymbol{B}_a &= \boldsymbol{B}_0 \left[\left(\frac{\beta\Delta t^2}{\gamma} - \frac{\Delta t^2}{2}\right)\boldsymbol{K} + \left(\frac{1}{\gamma}-1\right)\boldsymbol{I} \right] \end{aligned} \tag{5}$$

and

$$\begin{aligned} \boldsymbol{C}_0 &= \frac{1}{\beta\Delta t^2}A_0, \ \boldsymbol{C}_d = -\boldsymbol{C}_0\boldsymbol{K}, \\ \boldsymbol{C}_v &= -\boldsymbol{C}_0\left(\boldsymbol{C} + \Delta t\boldsymbol{K}\right), \\ \boldsymbol{C}_a &= \boldsymbol{C}_0 \left[(\gamma-1)\Delta t\boldsymbol{C} - \beta\Delta t^2\left(\frac{1}{2\beta}-1\right)\boldsymbol{K} \right]. \end{aligned} \tag{6}$$

Among them, β and γ are parameters of Newmark-β method.

According to the modal superposition method, the corresponding relationship between displacement in physical space and modal space, as well as the calculation formula for modal force, can be obtained. Therefore, the relationship between displacement and modal force in modal space (Eq. (3)) can be transformed into physical space, thereby establishing the convolution relationship between the response and the load in physical space [17].

$$\boldsymbol{Y} = \boldsymbol{H}\boldsymbol{F}, \tag{7}$$

where $\boldsymbol{H}=\begin{bmatrix} \boldsymbol{H}_1 & 0 & \cdots & 0 \\ \boldsymbol{H}_2 & \boldsymbol{H}_1 & \cdots & 0 \\ \vdots & \vdots & \ddots & \vdots \\ \boldsymbol{H}_z & \boldsymbol{H}_{z-1} & \cdots & \boldsymbol{H}_1 \end{bmatrix}$, $\boldsymbol{Y}=\begin{Bmatrix} \boldsymbol{y}(t_1) \\ \dot{\boldsymbol{y}}(t_1) \\ \ddot{\boldsymbol{y}}(t_1) \\ \vdots \\ \boldsymbol{y}(t_m) \\ \dot{\boldsymbol{y}}(t_m) \\ \ddot{\boldsymbol{y}}(t_m) \end{Bmatrix}$

$$\boldsymbol{F}=\begin{bmatrix} F_1(t_i) \\ F_2(t_i) \\ \vdots \\ F_n(t_i) \end{bmatrix}.$$

$\boldsymbol{Y}$ ($\boldsymbol{Y} \in \mathbb{R}^m$) is the output response, $\boldsymbol{F}$ ($\boldsymbol{F} \in \mathbb{R}^n$) is the load vector ($F_n(t_i)$ represents the n-th concentrated load

at time t_i), and $\boldsymbol{H}$ ($\boldsymbol{H} \in \mathbb{R}^{m\times n}$) is the transfer matrix; z represents the number of time instants.

To ensure Eq. (7) has a solution, the number of responses m should be greater than or equal to the modal order r, and the modal order r should be greater than or equal to the number of load identifications n. That is $m \geq r \geq n$. From Eq. (7), the load can be calculated as:

$$\boldsymbol{F} = \boldsymbol{H}^{+}\boldsymbol{Y} . \tag{8}$$

For continuous systems, infinite continuous systems can be transformed into finite degree of freedom systems through modal truncation. This reduction process ensures computational accuracy by retaining the dominant mode. Thus, the dynamic load identification method of multi degree of freedom systems can be used to complete the dynamic load identification of continuous systems.

3. Improved Hybrid LSQR Regularization Strategy for Dynamic Load Identification

However, the load identification problem (Eq. (8)) is an ill-posed inverse problem, which requires regularization strategies to enhance solution accuracy. The Least Squares QR (LSQR) algorithm is a commonly used regularization method. It solves linear systems and least squares problems through Lanczos bidiagonalization, making it particularly suitable for large-scale ill-posed problems.

The identification of dynamic loads requires consideration of the solution to the following least squares problem:

$$\min_{F\in\mathbb{R}^n} \left\| \boldsymbol{HF} - \boldsymbol{Y} \right\| . \tag{9}$$

Through the Lanczos diagonalization process based on the Krylov subspace projection method, the orthogonal bases of the subspaces $\kappa_k(\boldsymbol{H}^T\boldsymbol{H}, \boldsymbol{H}^T\boldsymbol{Y})$ and $\kappa_k(\boldsymbol{H}\boldsymbol{H}^T, \boldsymbol{Y})$ can be calculated respectively.

Let $\boldsymbol{F}_0$ be the initial approximate solution of Eq. (9), then the residuals $r_0 = \boldsymbol{Y} - \boldsymbol{H}\boldsymbol{F}_0$. After k steps of Lanczos diagonalization iteration, the bidiagonalization decomposition of matrix $\boldsymbol{H}$ was achieved:

$$\boldsymbol{H} \approx \boldsymbol{U}_{k+1}\boldsymbol{B}_k\boldsymbol{V}_k^T . \tag{10}$$

In which, two standard orthogonalization matrices are $\boldsymbol{V}_k = (v_1, v_2, \ldots, v_k) \in \mathbb{R}^{m\times k}$,

$\boldsymbol{U}_{k+1} = (u_1, u_2, \ldots, u_{k+1}) \in \mathbb{R}^{m\times(k+1)}$ and one diagonalization matrix is $\boldsymbol{B}_k = \begin{bmatrix} \alpha_1 & & & \\ \beta_2 & \alpha_2 & & \\ & \beta_3 & \ddots & \\ & & \ddots & \alpha_k \\ & & & \beta_{k+1} \end{bmatrix} \in \mathbb{R}^{(k+1)\times k}$.

The Lanczos diagonalization iteration process of the LSQR algorithm can be represented by a matrix as follows:

$$\begin{aligned} &\boldsymbol{U}_{k+1}(\beta_1 e_1) = \boldsymbol{Y}, \\ &\boldsymbol{H}\boldsymbol{V}_k = \boldsymbol{U}_{k+1}\boldsymbol{B}_k, \\ &\boldsymbol{H}^T\boldsymbol{U}_{k+1} = \boldsymbol{V}_k\boldsymbol{B}_k^T + \alpha_{k+1}v_{k+1}e_{k+1}^T . \end{aligned} \tag{11}$$

According to Eq. (8) and Eq. (10). the solution of LSQR algorithm is expressed as:

$$\boldsymbol{F}_k = \boldsymbol{V}_k\boldsymbol{B}_k^{+}\boldsymbol{U}_{k+1}^T\boldsymbol{Y} . \tag{12}$$

The LSQR algorithm exhibits semi-convergence [18]. To address this issue, Tikhonov regularization is incorporated into the least-squares problem within its subspace, resulting in a hybrid LSQR algorithm.

The solution vector $\boldsymbol{F}_k$ lies in the column space of $\boldsymbol{V}_k$. In the LSQR algorithm, the solution is approximated as $\boldsymbol{F}_k = \boldsymbol{V}_k q_k$, which corresponds to the residual $r_k = \boldsymbol{Y} - \boldsymbol{H}\boldsymbol{F}_k$.

Define $t_{k+1} = \beta_1 e_1 - \boldsymbol{B}_k q_k$, we can get:

$$\begin{aligned} r_k &= \boldsymbol{Y} - \boldsymbol{H}\boldsymbol{F}_k = \boldsymbol{U}_{k+1}(\beta_1 e_1) - \boldsymbol{H}\boldsymbol{V}_k q_k = \\ &= \boldsymbol{U}_{k+1}(\beta_1 e_1) - \boldsymbol{U}_{k+1}\boldsymbol{B}_k q_k = \boldsymbol{U}_{k+1}t_{k+1}. \end{aligned} \tag{13}$$

The minimum residual r_k is equivalent to solving q_k to minimize $\|t_{k+1}\|$. That is:

$$\min\left\|t_{k+1}\right\| = \left\|\beta_1 e_1 - \boldsymbol{B}_k q_k\right\| = \left\|\boldsymbol{U}_{k+1}^T\boldsymbol{Y} - \boldsymbol{B}_k q_k\right\| . \tag{14}$$

Tikhonov regularization is incorporated into the least-squares problem, we get:

$$\min\left\{\left\|\boldsymbol{U}_{k+1}^T\boldsymbol{Y} - \boldsymbol{B}_k q_k\right\| + \lambda^2\left\|q_k\right\|\right\} , \tag{15}$$

where λ is the regularization parameter obtained through the L-curve criterion [19], The idea of this method is to select a series of different λ values, compute the corresponding values of $lg\|Y–HF\|$ and $lg\|F\|$ for each λ respectively. Plot a graph with $lg\|Y–HF\|$ as the abscissa and $lg\|F\|$ as the ordinate, whose curve shape resembles the letter "L". At the corner of the L-curve, the point with the maximum curvature can be found, and the λ value corresponding to this point is the most suitable regularization parameter. The Tikhonov regularization solution in the subspace is:

$$q_k^R = \left(\boldsymbol{B}_k^T\boldsymbol{B}_k + \lambda^2\boldsymbol{I}\right)^{-1}\boldsymbol{B}_k^T\boldsymbol{U}_{k+1}^T\boldsymbol{Y} . \tag{16}$$

The load identified by the hybrid LSQR algorithm is:

$$\boldsymbol{F}_k^R = \boldsymbol{V}_k q_k^R = \boldsymbol{V}_k\left(\boldsymbol{B}_k^T\boldsymbol{B}_k + \lambda^2\boldsymbol{I}\right)^{-1}\boldsymbol{B}_k^T\boldsymbol{U}_{k+1}^T\boldsymbol{Y} . \tag{17}$$

The hybrid LSQR algorithm solves the smaller-scale regularization problem on the low-dimensional subspace generated by the original LSQR algorithm, thereby achieving the goal of performing refined regularization for large-scale sparse problems. To enhance the accuracy and stability of the hybrid LSQR algorithm, this paper proposes an improved version. The computed load obtained through

the hybrid LSQR algorithm is adjusted based on the deviation between the calculated response and the measured response. The solution of the improved hybrid LSQR algorithm is expressed as:

$$\begin{aligned} \boldsymbol{F}_k^M &= \boldsymbol{F}_k^R + \mu\Delta\boldsymbol{F}_k = \boldsymbol{V}_k q_k^R + \mu\boldsymbol{V}_k\Delta q_k = \\ &= \boldsymbol{V}_k\left(q_k^R + \mu\boldsymbol{B}_k^R\boldsymbol{U}_{k+1}^T\Delta\boldsymbol{Y}\right), \end{aligned} \tag{18}$$

where, μ is the correction coefficient, $\Delta\boldsymbol{F}_k$ is the deviation between the hybrid LSQR solution and the actual load at the k-th step, and $\Delta\boldsymbol{Y} = \boldsymbol{Y} - \boldsymbol{H}\boldsymbol{F}_k^R$, $\boldsymbol{H}\boldsymbol{F}_k^R$ is the calculated response. the deviation between the measured response and the calculated response is:

$$\begin{aligned} \Delta\boldsymbol{Y}^m &= \boldsymbol{Y} - \boldsymbol{H}\left(\boldsymbol{F}_k^R + \mu\Delta\boldsymbol{F}_k\right) = \\ &= \Delta\boldsymbol{Y} - \mu\boldsymbol{U}_{k+1}\boldsymbol{B}_k\boldsymbol{B}_k^R\boldsymbol{U}_{k+1}^T\Delta\boldsymbol{Y}\ . \end{aligned} \tag{19}$$

The objective function is defined as the difference between the measured response and the calculated response:

$$\omega(\mu) = \left\|\Delta\boldsymbol{Y}^m\right\|^2 = \left\|\Delta\boldsymbol{Y} - \mu\boldsymbol{U}_{k+1}\boldsymbol{B}_k\boldsymbol{B}_k^R\boldsymbol{U}_{k+1}^T\Delta\boldsymbol{Y}\right\|^2 . \tag{20}$$

Let the partial derivative of $\omega(\mu)$ with respect to μ be zero, resulting in:

$$\mu = \frac{\left(\boldsymbol{U}_{k+1}\boldsymbol{B}_k\boldsymbol{B}_k^R\boldsymbol{U}_{k+1}^T\Delta\boldsymbol{Y}\right)^T\Delta\boldsymbol{Y}}{\left\|\boldsymbol{U}_{k+1}\boldsymbol{B}_k\boldsymbol{B}_k^R\boldsymbol{U}_{k+1}^T\Delta\boldsymbol{Y}\right\|^2} . \tag{21}$$

By substituting Eq. (21) into Eq. (18), the k-th iterative regularization solution of the improved hybrid LSQR algorithm can be obtained. The flowchart of load identification using the improved hybrid LSQR algorithm is shown in Fig. 2.

4. Augmented Hybrid LSQR Regularization Strategy for Dynamic Load Identification

The improved hybrid LSQR algorithm is derived by integrating the LSQR method with Tikhonov regularization. The solution produced by the LSQR algorithm resides within the Krylov subspace. However, the standard Krylov subspace does not incorporate prior knowledge about the load. To address this limitation in applications where such information is available, an Augmented Hybrid LSQR Algorithm is proposed.

If it is known that the load signal $\boldsymbol{F}$ contains a subspace w_p, the solution can be obtained by solving the following least squares problem:

$$\min_{\boldsymbol{F}\in\mathbb{R}^n}\left\|\boldsymbol{H}\boldsymbol{F} - \boldsymbol{Y}\right\| \quad s.t. \quad \boldsymbol{F} \in \kappa_k + w_p\ . \tag{22}$$

The LSQR algorithm Lanczos diagonalization iteration process becomes:

$$\boldsymbol{H}\left[\boldsymbol{V}_k, w_P\right] = \left[\boldsymbol{U}_{k+1}, \tilde{\boldsymbol{U}}_k\right]\begin{bmatrix}\boldsymbol{B}_k & \boldsymbol{G}_k\\ 0 & \boldsymbol{F}_k\end{bmatrix}, \tag{23}$$

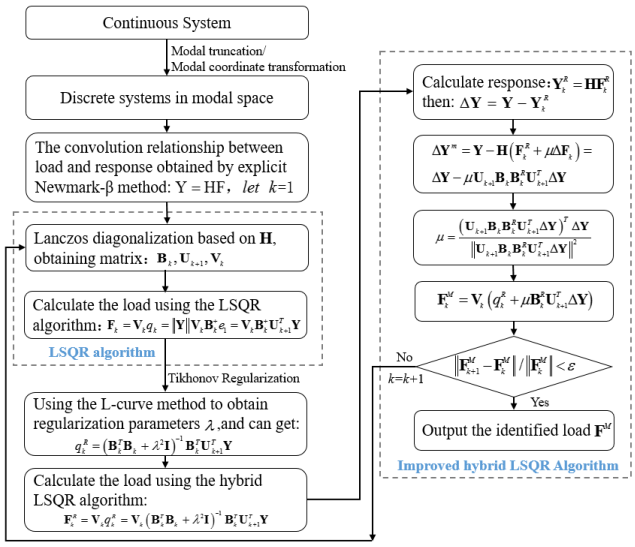

Fig. 2 Flowchart of load identification using improved hybrid LSQR algorithm

where, $\tilde{\boldsymbol{U}}_k \in \mathbb{R}^{m\times p}$, $\tilde{\boldsymbol{U}}_k^T\boldsymbol{U}_{k+1} = 0$,
$range\left(\boldsymbol{H}w_p\right) = range\left(\boldsymbol{U}_{k+1}\boldsymbol{G}_k + \tilde{\boldsymbol{U}}_k\boldsymbol{F}_k\right)$. $\boldsymbol{G}_k \in \mathbb{R}^{(k+1)\times p}$, $\boldsymbol{F}_k \in \mathbb{R}^{p\times p}$, and the expression for $\boldsymbol{G}_k$, $\boldsymbol{F}_k$ are as follows:

$$\boldsymbol{G}_k = \boldsymbol{U}_{k+1}^T\boldsymbol{H}w_p\ , \quad \boldsymbol{F}_k = \tilde{\boldsymbol{U}}_k^T\boldsymbol{H}w_p\ . \tag{24}$$

Iterate k steps to obtain an approximate solution $\boldsymbol{F}_k = [\boldsymbol{V}_k, w_p]q_k$ for the augmented hybrid LSQR algorithm, where q_k is the solution to the following least squares problem:

$$min_q\left\{\left\|\bar{\boldsymbol{B}}_k q_k - \bar{\boldsymbol{U}}_{k+1}^T\boldsymbol{Y}\right\|\right\}, \tag{25}$$

in which, $\bar{\boldsymbol{B}}_k = \begin{bmatrix}\boldsymbol{B}_k & \boldsymbol{G}_k\\ 0 & \boldsymbol{F}_k\end{bmatrix}$, $\bar{\boldsymbol{U}}_k = \left[\boldsymbol{U}_{k+1}, \tilde{\boldsymbol{U}}_k\right]$. Using Tikhonov regularization to solve the least squares problem of Eq. (15), we obtain:

$$min\left\{\left\|\bar{\boldsymbol{B}}_k q_k - \bar{\boldsymbol{U}}_{k+1}^T\boldsymbol{Y}\right\| + \lambda^2\left\|q_k\right\|\right\}. \tag{26}$$

The Tikhonov regularization in the subspace is resolved as follows:

$$q_k^R = \left(\bar{\boldsymbol{B}}_k^T\bar{\boldsymbol{B}}_k + \lambda^2\boldsymbol{I}\right)^{-1}\bar{\boldsymbol{B}}_k^T\bar{\boldsymbol{U}}_{k+1}^T\boldsymbol{Y}\ . \tag{27}$$

According to the improved hybrid LSQR algorithm, the identified load is modified. and the augmented hybrid LSQR algorithm solution can be obtained:

$$\begin{aligned} \boldsymbol{F}_k &= \boldsymbol{F}_k^R + \mu\Delta\boldsymbol{F}_k = \left[\boldsymbol{V}_k, w_p\right]q_k^R + \mu\left[\boldsymbol{V}_k, w_p\right]\Delta q_k = \\ &= \left[\boldsymbol{V}_k, w_p\right]\left(q_k^R + \mu\bar{\boldsymbol{B}}_k^R\bar{\boldsymbol{U}}_{k+1}^T\Delta\boldsymbol{Y}\right), \end{aligned} \tag{28}$$

where $\bar{\boldsymbol{B}}_k^R = \left(\bar{\boldsymbol{B}}_k^T\bar{\boldsymbol{B}}_k + \lambda^2\boldsymbol{I}\right)^{-1}\bar{\boldsymbol{B}}_k^T$,

$\mu = \dfrac{\left(\bar{\boldsymbol{U}}_{k+1}\bar{\boldsymbol{B}}_k\bar{\boldsymbol{B}}_k^R\bar{\boldsymbol{U}}_{k+1}^T\Delta\boldsymbol{Y}\right)^T\Delta\boldsymbol{Y}}{\left\|\bar{\boldsymbol{U}}_{k+1}\bar{\boldsymbol{B}}_k\bar{\boldsymbol{B}}_k^R\bar{\boldsymbol{U}}_{k+1}^T\Delta\boldsymbol{Y}\right\|^2}$, $\Delta\mathbf{Y} = \mathbf{Y} - \mathbf{Y}^+$, and $\boldsymbol{Y}^+ = \boldsymbol{H}\boldsymbol{F}_k^R$.

Using the augmented hybrid LSQR algorithm to perform iterative calculations, dynamic loads with known prior information can be effectively identified. Figure 3 presents the corresponding flowchart for this load identification process.

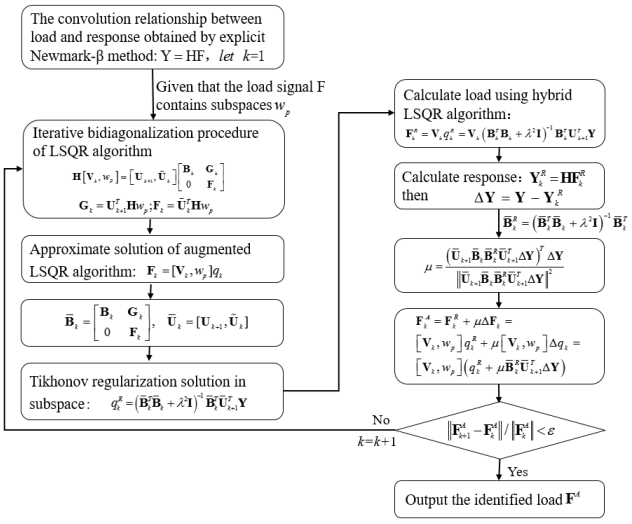

Fig. 3 Flowchart of load identification using augmented hybrid LSQR algorithm

5. Simulation Example

Using finite element software to establish a simply supported beam model with length $l = 1$ m, width $a = 0.05$ m, and height $h = 0.01$ m. With elastic modulus $E = 210$ GPa, density $\rho = 7800$ kg/m^3, and Poisson's ratio $\mu = 0.3$. The finite element model of the simply supported beam is shown in Fig. 4.

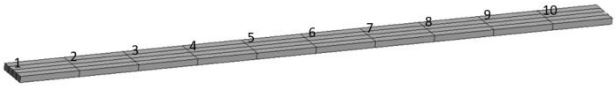

Fig. 4 Finite element model of simply supported beam

5.1. Evaluation of dynamic load identification

This study employs the Signal-to-Noise Ratio (SNR) and the Peak Relative Error Method (PREM) to evaluate the discrepancy between the actual load $X(i)$ and the identified load $Y(i)$.

1. Signal-to-Noise Ratio (SNR)

$$\mathrm{SNR}(X,Y) = 10\log_{10}\left(\frac{\sum_{i=1}^{n}X(i)^2}{\sum_{i=1}^{n}\left[X(i)-Y(i)\right]^2}\right), \qquad (27)$$

where, n is the number of sampling points. SNR quantifies the global discrepancy between the identified and actual loads. A higher and lower SNR indicates a smaller and larger identification error, respectively.

2. Peak relative error method (PREM)

$$\mathrm{PREM}(X,Y) = \frac{\left|max\,Y(i) - max\,X(i)\right|}{max\,X(i)} \times 100\%. \qquad (28)$$

PREM denotes the relative error between the peak value of the identified load and the peak value of the actual load.

5.2. Improved hybrid LSQR algorithm for multi-point sinusoidal excitation load identification

This example involves multi-point excitation, where multiple sinusoidal loads $F_1 = 20sin(80\pi t)$ and $F_2 = 10sin(60\pi t+\pi)$ are applied. The excitation points are at nodes 4 and 9, specifically, sinusoidal excitations are applied at $x_1 = 0.3$ m and $x_2 = 0.8$ m, respectively. Transient response analysis is performed using Patran, with external load signals and response signals from nodes 2–8 collected. The sampling rate is set to 2000 Hz, and a 1-second duration is selected for load identification analysis. For a simply supported beam with zero initial conditions, the modal truncation order is set to 5. The multi-source signal is shown in Fig. 5.

Gaussian white noise interference with intensities of 10% and 20% is added to the acceleration response signal, respectively. The identification results of the multi-point sinusoidal loads are presented in Figs. 6 and 7.

According to Table 1 and Table 2, as the noise increases, the PREM values of the two algorithms gradually increases, and the SNR values gradually decreases, indicating that noise has a significant interference on load identification. Comparing the identification of two sinusoidal loads using different algorithms, the load 2 has a larger identification error than the load 1. With the increase of noise, the identification accuracy of LSQR algorithm suddenly decreases, especially for the load 2 with 20% noise interference, whose PREM is as high as 112.738%. LSQR algorithm has poor noise resistance and low accuracy for multi-point sinusoidal load identification. Compared to the LSQR algorithm, the proposed improved hybrid LSQR algorithm exhibits enhanced robustness to noise, with lower PREM and higher SNR.

5.3. Simulation example of superposition load identification using augmented hybrid LSQR algorithm

The simulation model is consistent with the above example, as illustrated in Fig. 1. A superposition of a sinusoidal load and a linear load $F = 20sin(60\pi t)–10t$ is applied at node 4 (i.e., $x = 0.3$ m) for 0.5 seconds to conduct load identification and analysis. The modal truncation order is set to 3, and the applied load signal is presented in Fig. 8.

Assuming that the load contains linearly varying forces:

$w_p = span\{w_1, w_2\}$, $w_1 = (1, 1, \ldots, 1)^T$, $w_2 = (1, 2, \ldots, n)^T$.

To account for the influence of noise interference, 10% and 20% Gaussian white noise are added to the acceleration response, respectively. The corresponding load identification results are shown in Fig. 9 and Fig.10.

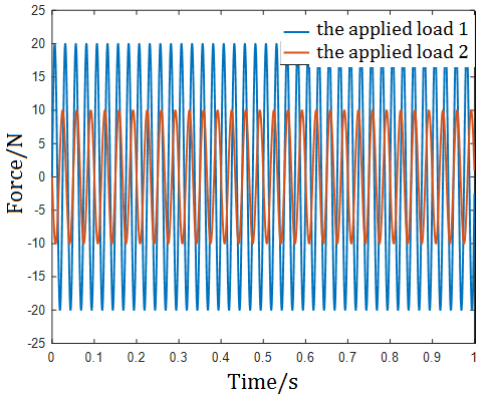

Fig. 5 Multi-point sinusoidal load excitation signal

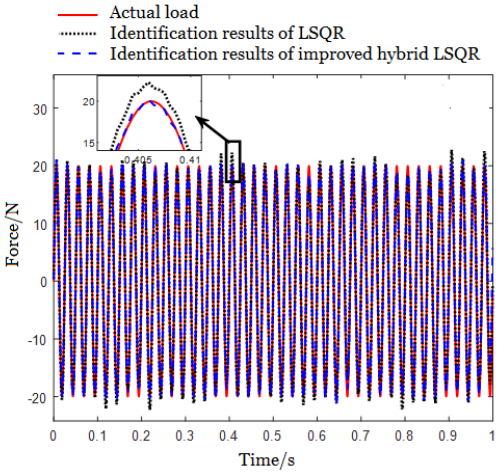

a

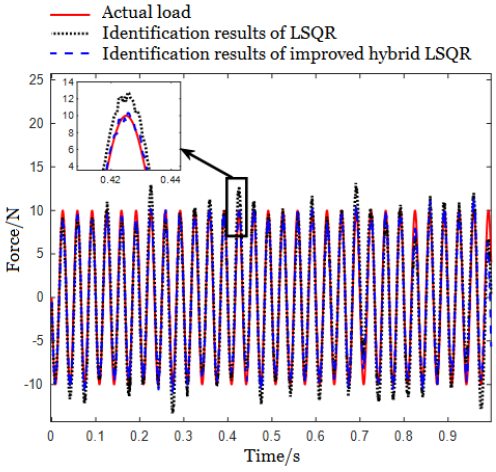

b

Fig. 6 Identification results of multi-point sinusoidal load with 10% noise interference: a – load 1, b – load 2

Table 1

Identification results of multi-point sinusoidal load (Load 1)

Algorithm	Noise	PRE (%)	SNR
LSQR Algorithm	10%	20.477	17.343
Improved Hybrid LSQR Algorithm		7.222	21.135
LSQR Algorithm	20%	41.624	11.507
Improved Hybrid LSQR Algorithm		18.179	16.461

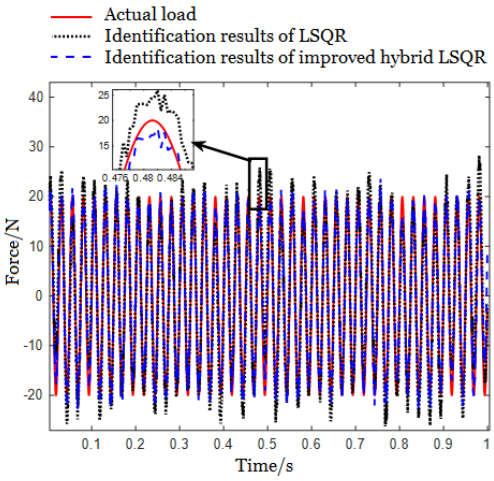

a

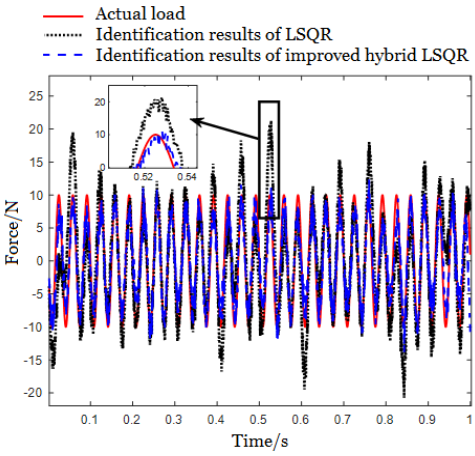

b

Fig. 7 Identification results of multi-point sinusoidal load with 20% noise interference: a – load 1, b – load 2

Table 2

Identification results of multi-point sinusoidal load (Load 2)

Algorithm	Noise	PRE (%)	SNR
LSQR Algorithm	10%	65.871	9.153
Improved Hybrid LSQR Algorithm		18.512	12.667
LSQR Algorithm	20%	112.738	3.421
Improved Hybrid LSQR Algorithm		38.265	8.436

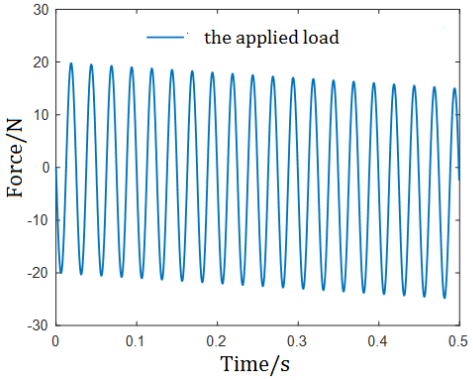

Fig. 8 Superposition excitation signal of sinusoidal load and linear load

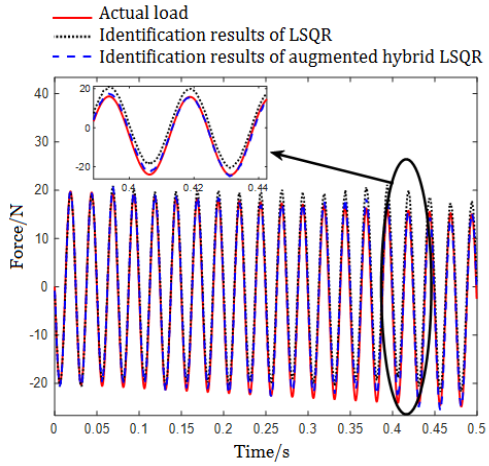

Fig. 9 Identification results of superposition load with 10% noise

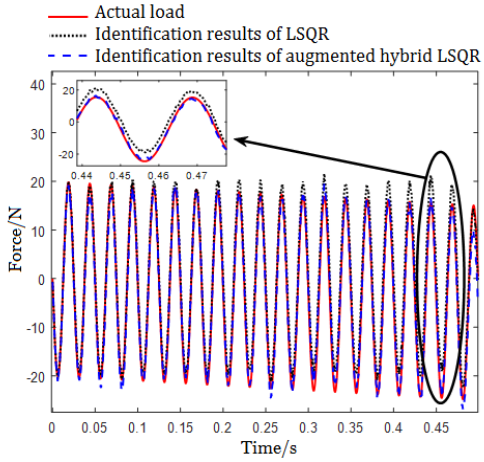

Fig. 10 Identification results of superposition load with 20% noise

As can be seen from Figs. 9-10, with different noise levels, the LSQR algorithm can only identify sinusoidal load but fails to identify linear load, resulting in significant errors in the identification results. In contrast, the augmented hybrid LSQR algorithm, based on known prior information, can effectively identify the superimposed load composed of sinusoidal and linear load.

Table 3
Identification results of multi-point sinusoidal load

Algorithm	Noise	PRE (%)	SNR
LSQR Algorithm	10%	12.288	14.370
Augmented Hybrid LSQR Algorithm		3.844	23.025
LSQR Algorithm	20%	9.808	13.936
Augmented Hybrid LSQR Algorithm		8.561	19.634

As can be seen from Table 3, with different noise levels, the LSQR algorithm exhibits large errors in identifying the composite load consisting of a sinusoidal load and a linear load. In contrast, the augmented hybrid LSQR algorithm achieves favorable identification results, with all SNR exceeding 19, indicating that this algorithm maintains good stability during the iteration process.

6. Experimental Verification of Periodic Load Identification Using Improved Hybrid LSQR Algorithm

Fig. 11 illustrates a low-carbon steel beam under a configuration with one fixed end and one simply supported end. The beam's nominal dimensions are a length of 0.7 m, a width of 0.04 m, and a thickness of 0.008 m.

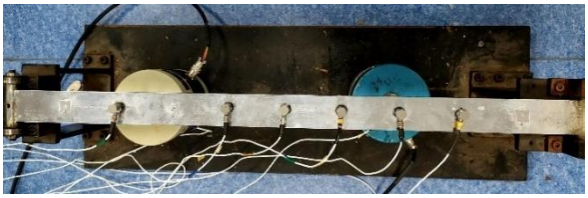

Fig. 11 Diagram of the simply supported beam in the dynamic response test

Perform load identification calculations using the acceleration response signal as input, and compare the identified load with the measured excitation load. The acceleration response at each measurement point under periodic excitation is collected, providing both the response data and the excitation data for load identification. Data was acquired using an NI-PXIe-1075 system and processed with the NI SignalExpress analysis software. When multiple excitations are applied, periodic loads are exerted using shakers.

The sampling rate is set to 2048 Hz, and acceleration responses are collected at six measurement points. The two periodic loads applied and the positions where they are applied are as follows:

$$x_1 = 0.21 \text{ m},\ F_1 = \sum_{k=0}^{10} 23\,sin\left[2\pi\left(40+10k\right)t\right],$$

$$x_2 = 0.56 \text{ m},\ F_2 = sin\left(160\pi t\right).$$

For load identification, a 1-second stationary segment of the excitation signal is intercepted as the analysis data. The identification results for the periodic loads under multiple excitations are presented in Fig. 12 and Fig. 13.

The performance of the multi-periodic load identification is presented in Table 4.

As shown in Figs. 12 and 13, significant errors are observed during the initial identification phase (within the first 0.03 seconds). After this period, the favorable Peak

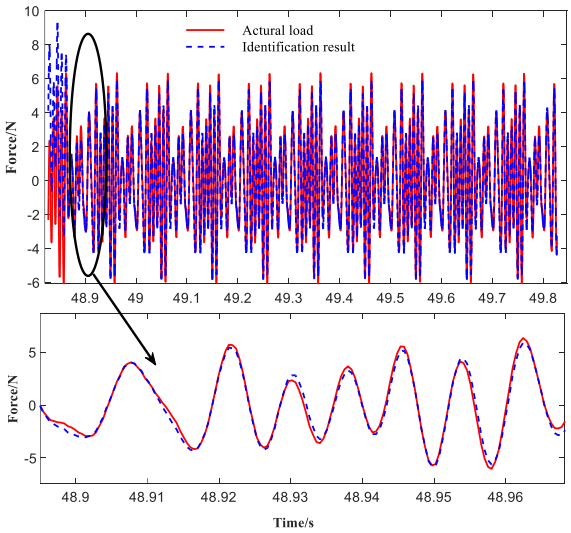

Fig. 12 Identification results of F_1

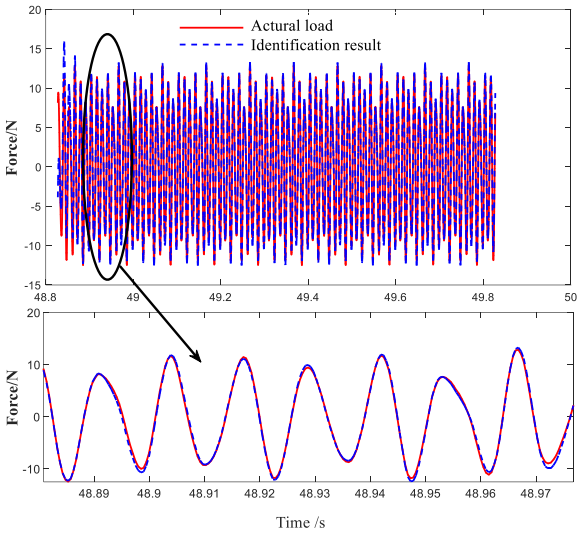

Fig. 13 Identification results of F_2

Relative Error (PREM) and Signal-to-Noise Ratio (SNR) values, presented in Table 4, indicate effective load identification. The large initial error is primarily attributed to neglecting the influence of prior excitation on the current response when analyzing the data segment.

Table 4
Identification Results of Multi-periodic Load

Multi-source periodic excitation loads	PRE, %	SNR
F_1	7.037	17.045
F_2	3.132	24.510

7. Conclusions

This paper employs the explicit Newmark-β method for load identification in continuous systems. Addressing the ill-posed nature inherent in load identification, an improved hybrid LSQR regularization strategy is proposed. For load identification problems with prior conditions, an augmented hybrid LSQR regularization strategy is further developed. The stability and accuracy of these two methods are validated through simulation examples. The main contributions of this work are as follows:

Based on the LSQR regularization algorithm, an improved hybrid LSQR algorithm is proposed. This approach incorporates an adaptive correction mechanism, where the computed response is iteratively compared with the measured response. Numerical simulations confirm that the proposed improved hybrid LSQR algorithm exhibits superior stability and accuracy compared to the conventional LSQR algorithm.

In cases where prior information is accessible, an augmented hybrid LSQR algorithm is proposed. the augmented hybrid LSQR algorithm expands the Krylov subspace with prior information and combines improved hybrid LSQR regularization strategies to ensure stable iteration, enabling it to better handle dynamic load identification problems with prior information.

Using a simply supported beam as a representative structure of a continuous system, simulation examples involving different load types and noise levels demonstrate that the improved hybrid LSQR algorithm yields relatively favorable identification results. Additionally, a superposition load identification simulation shows that the augmented hybrid LSQR algorithm further improves the accuracy of load identification when prior knowledge of the load is available. Finally, the reliability and accuracy of the hybrid LSQR correction algorithm in identifying periodic loads are verified through experimentation.

Acknowledgement

This research is supported by the National Natural Science Foundation of China (No. 12372066 & No. U23B6009) and Foundation of National Key Laboratory of Science and Technology on Rotorcraft Aeromechanics (No. 61422202105), Qing Lan Project and National Natural Science Foundation of China (No. 52171261).

References

1. **Fu, D.; Wang, L.; Lv, G.; Shen, Z.; Zhu, H.; Zhu, W.D.** 2023. Advances in dynamic load identification based on data-driven techniques, Engineering Applications of Artificial Intelligence 126: 106871. https://doi.org/10.1016/j.engappai.2023.106871.
2. **Liu, R.; Dobriban, E.; Hou, Z.; Qian, K.** 2021. Dynamic Load Identification for Mechanical Systems: A Review, Archives of Computational Methods in Engineering 29(2): 831-863. https://doi.org/10.1007/s11831-021-09594-7.
3. **Li, H.; Jiang, J.; Mohamed M S. 2025.** Study on Simultaneous Identification of External Excitation and Response Reconstruction for Continuous System, Mechanika 31(1): 35-43. https://doi.org/10.5755/j02.mech.38958.
4. **Qin, Y.; Zhang, Y.; Silberschmidt, V.; Zhang, L.** 2023. Method for Dynamic Load Location Identification Based on FRF Decomposition, Aerospace 10(10): 852. https://doi.org/10.3390/aerospace10100852.
5. **Kulkarni, R. B.; Gopalakrishnan, S.; Trikha, M.** 2020. Impact force identification in structures using time-domain spectral finite elements, Acta Mechanica 231(11): 4513–4528. https://doi.org/10.1007/s00707-020-02775-8.
6. **Yuen, K.V.; Guo, H.Z.; Mu, H.Q.** 2023. Bayesian Vehicle Load Estimation, Vehicle Position Tracking, and Structural Identification for Bridges with Strain Measurement, Structural Control and Health Monitoring 2023(1): 4752776. https://doi.org/10.1155/2023/4752776.
7. **Pourzeynali, S.; Zhu, X.; Ghari Zadeh, A.; Rashidi, M.; Samali, B.** 2021. Comprehensive Study of Moving Load Identification on Bridge Structures Using the Explicit Form of Newmark-β Method: Numerical and Experimental Studies, Remote Sensing 13(12): 2291. https://doi.org/10.3390/rs13122291.
8. **Cheng, Y.; Li, Z.; Zhang, L.; Jiang, M.; Wang, S.; Sui, Q.; Jia, L.;** 2023. Multi-type dynamic load identification algorithm in continuous system: A numerical and experimental study based on SSM-Newmark-β, Applied Mathematical Modelling 123: 810-834. https://doi.org/10.1016/j.apm.2023.07.010.
9. **Yu, X.; Cheng, C.; Yang, Y.; Du, M.; He, Q.; Peng, Z.K.** 2023. Maximumly weighted iteration for solving inverse problems in dynamics, International Journal of

Mechanical Sciences 247: 108169. https://doi.org/10.1016/j.ijmecsci.2023.108169.
10. **Carević, A.; Slapničar, I.; Almekkawy, M.** 2022. Solving Ultrasound Tomography's Inverse Problem: Automating Regularization Parameter Selection, IEEE Transactions on Ultrasonics, Ferroelectrics, and Frequency Control 69(8): 2447-2461. https://doi.org/10.1109/tuffc.2022.3182147.
11. **Wang, L.; Xu, H.; Liu, Y.** 2023. A novel dynamic load identification approach for multi-source uncertain structures based on the set-theoretical wavelet transform and layered noise reduction, Structures 51: 91-104. https://doi.org/10.1016/j.istruc.2023.03.037.
12. **Hanke, M.** 2001. On Lanczos Based Methods for the Regularization of Discrete Ill-Posed Problems, Bit Numerical Mathematics 41(5): 1008-1018. https://doi.org/10.1023/A:1021941328858.
13. **Baglama, J.; Reichel, L.; Richmond, D.** 2012. An augmented LSQR method, Numerical Algorithms 64(2): 263-293. https://doi.org/10.1007/s11075-012-9665-8.
14. **Asgari, Z.; Toutounian, F.; Babolian, E.** 2020. Augmented Subspaces in the LSQR Krylov Method, Iranian Journal of Science and Technology, Transactions A: Science 44(6): 1661-1665. https://doi.org/10.1007/s40995-020-01002-2.
15. **Saha, S.** 2025. Physics Informed Neural Networks for Dynamic Load Reconstruction for Plant Piping, International Journal for Multidisciplinary Research 7(1): 36918. https://doi.org/10.36948/ijfmr.2025.v07i01.36918.
16. **Cui, W.; Jiang, J.; Sun, H.; Yang, H.; Wang, X.; Wang, L.; Li, H.** 2023. Data-driven load identification method of structures with uncertain parameters, Acta Mechanica Sinica 40: 523138. https://doi.org/10.1007/s10409-023-23138-x.
17. **Jiang, J.; Ding, M.; Li, J.** 2021. A novel time-domain dynamic load identification numerical algorithm for continuous systems, Mechanical Systems and Signal Processing 160: 107881. https://doi.org/10.1016/j.ymssp.2021.107881.
18. **Miao, B.; Zhou, F.; Chen, X.; Yang, S.; Li, X.** 2018. Research of the structure load identification hybrid technology using kernel function and different regularization methods, Journal of Vibration Engineering 31(4): 553-560. https://doi.org/10.16385/j.cnki.issn.1004-4523.2018.04.002.
19. **Li, X.; Zhao, H.; Chen, J.** 2020. Force identification Based on Measuring Point Selection and Improved L-Curve Method, Journal of Shanghai Jiaotong University 54(6): 569-576. https://doi.org/10.16183/j.cnki.jsjtu.2019.016.

H. Li, J. Jiang, M S. Mohamed

RESEARCH ON DYNAMIC LOAD IDENTIFICATION BASED ON THE NEWMARK-β METHOD AND NOVEL ITERATIVE REGULARIZATION STRATEGY

S u m m a r y

This work focuses on the dynamic load identification motivated by Newmark-β Method and regularization strategy. Given the ill-posed nature of load identification, an improved hybrid LSQR regularization strategy is proposed, which incorporates an adaptive correction mechanism by iteratively comparing the computed response with the measured response. For load identification problems with prior conditions, an augmented hybrid LSQR regularization strategy is further developed, which expands the Krylov subspace with prior information and combines the improved hybrid LSQR regularization strategies to ensure stable iteration. Simulation examples using a simply supported beam as a representative structure of continuous systems, involving different load types and noise levels, validate the stability and accuracy of the two methods. The results show that the improved hybrid LSQR algorithm exhibits its superior stability and accuracy compared to the conventional LSQR algorithm and yields relatively favorable identification results. Moreover, the superposition load identification simulation indicates that the augmented hybrid LSQR algorithm further improves the accuracy of load identification when prior knowledge of the load is available.

Keywords: dynamic load identification, explicit Newmark-β method, regularization strategy, improved hybrid LSQR algorithm, augmented hybrid LSQR algorithm.

Received September 6, 2025
Accepted April 24, 2026